

NASA Contractor Report 179644

# SSME Single Crystal Turbine Blade Dynamics

(NASA-CR-179644) SSME SINGLE CRYSTAL

TURBINE BLADE DYNAMICS Final Report

(Sverdrup Technology) 27 p Avail: NTIS HC

A03/MF A01

CSCI 20K

N87-26384

Unclass

G3/39 0085261

Larry A. Moss and Todd E. Smith

*Sverdrup Technology, Inc.*

*Lewis Research Center*

*Cleveland, Ohio*

July 1987

Prepared for

Lewis Research Center

Under Contract NAS3-24105



National Aeronautics and  
Space Administration

## SSME SINGLE CRYSTAL TURBINE BLADE DYNAMICS

Larry A. Moss and Todd E. Smith  
Sverdrup Technology Inc.  
Lewis Research Center  
Cleveland, Ohio 44135

### SUMMARY

A study was performed to determine the dynamic characteristics of the Space Shuttle main engine (SSME) high pressure fuel turbopump (HPFTP) blades made of single crystal (SC) material. This effort examined both the first and second stage drive turbine blades of the HPFTP. The nonrotating natural frequencies were determined experimentally and analytically. The experimental results of the SC second stage blade were used to verify the analytical procedures. The analytical study examined the SC first stage blade natural frequencies with respect to crystal orientation at typical operating conditions. The SC blade dynamic response was predicted to be less than the directionally solidified (DS) blade. No new engine order interferences were introduced and one was eliminated. Crystal axis orientation optimization indicated the third mode interference will exist at any SC orientation.

### INTRODUCTION

There are many concerns surrounding the current SSME first stage HPFTP blades made of directionally solidified (DS) MAR-M-246 + Hf material. The blades' design life goal was 55 launches (ref. 1). However, the DS blades have been serviceable for only two to five launches. The shortened service life results in a significant cost in refurbishing a shuttle for its next flight. Replacement costs of the DS blades only account for about 7 percent of the total reblading costs. Reassembly and testing expenditures account for more than half of the total reblading costs. Improving the blade life will reduce both time and money required for maintaining and reblading the pump.

The blade life is being shortened due to cracking caused from a combination of both low cycle fatigue (LCF) and high cycle fatigue (HCF). The LCF is a result of the DS blades exposure to severe thermal transients. Temperatures range from a cryogenic atmosphere before start up, to a maximum of about 2350°F, with a steady-state operating temperature of 1550 °F. HCF results from lower amplitude vibratory stress, superimposed upon high steady stress.

One method of improving blade life is with an advanced casting process. Past experience and current applications with commercial and military aviation have shown it is feasible and advantageous to manufacture blades with one crystal, known as single crystal (SC) material. The SC material eliminates all grain boundaries within the blade. The exclusion of grain boundaries has essentially eliminated a fatigue failure mechanism associated with grain boundary separation. Therefore, the SC material properties (fatigue and creep) are improved over those of the DS material and are more resistant to the severe operating demands of the turbopump blades.

## BACKGROUND

There are 63 SSME HPFTP blades mounted within the first stage rotor (fig. 1). The mounted blades have a tip diameter of approximately 11 in. (ref. 2). The blades consist of four sections; airfoil, platform, shank, and fir tree (fig. 2). The airfoil is highly cambered and the cross section is nearly constant along the slightly twisted blade span. The four-lobed fir tree section mates with the rotor.

The SC material orientation is determined from Laue' X-RAY Diffraction Techniques. Polar projections of the material's  $\langle 111 \rangle$  axis, are developed. The  $\langle 111 \rangle$  axis is referenced within the HPFTP blade according to its projected "rotate" angle and "tilt" angle. The tilt angle is measured between the  $111$  axis and the blade's span direction. The rotation angle is referenced according to the  $\langle 111 \rangle$  axis projection on the X-Y plane of the blade. Positive rotation is measured counterclockwise from the blade chord (leading edge to trailing edge) with respect to the trailing edge (fig. 3).

The crystal growth direction is along the material  $\langle 001 \rangle$  axis. When the  $\langle 001 \rangle$  axis is exactly aligned in the blade's span direction, the tilt angle is at  $54.74^\circ$  (fig. 3). The solidification direction along the  $\langle 001 \rangle$  axis is the same as the DS blade material.

## APPROACH

The purpose of this preliminary evaluation was to predict the SC blade natural frequencies and find possible critical engine order excitations. This investigation was a limited scope study and was not intended to be detailed study. This study examined both the first and second stage drive turbine blades of the HPFTP. The effort was both experimental and analytical.

Experiments were used to validate the analytical procedures. Only SC second stage blades were available. Bench experiments for five SC MAR-M-246 + Hf second stage blades at different crystal orientations were conducted to determine their nonrotating natural frequencies and mode shapes. Comparisons of these results with the analytical results were made to confirm the validity of the MSC/NASTRAN model of the second stage blade.

The first and second stage finite element models were similar as far as finite element method, element types, and boundary conditions. Therefore, it was assumed that validation of the second stage blade model would be sufficient for the first stage blade model.

The analytical effort examined the SC PWA-1480 first stage HPFTP blade dynamic characteristics with respect to crystal orientations under typical operating conditions. Two operating conditions, 27 500 and 35 000 rpm, were investigated. Each speed had a unique blade temperature distribution. Additional investigations attempted to determine optimum crystal orientations which would most effectively avoid critical engine order excitations.

## EXPERIMENTAL PROCEDURES

To simulate the blade in the actual rotor, the SC blades were brazed in a stainless steel block (fig. 4). The fir tree lobes were ground smooth to fit into a tapered channel in the block. This gave an excellent brazing surface for bonding purposes. A rigid attachment was achieved by flowing a braze type flux material, PAL-NIRO-1, around the area of the fir tree.

Five SC MAR-M-246 + Hf second stage blades were tested. Each blade had a different crystal orientation as listed in table I. The tests were conducted at nonrotating, room temperature conditions. Two experimental methods were used to identify the modal frequencies and approximate the mode shapes of the SC blades. These methods involved a modal analyzer and interferometry.

### FFT Modal Analyzer

Testing was performed with the aid of a Hewlett Packard HP 5423A FFT Modal Analyzer (fig. 5). A magnetic chip was attached to the blade airfoil tip and excited by an electromagnetic coil. The blade response was measured by an accelerometer attached to the blade tip trailing edge. The chip and accelerometer locations were chosen to obtain strong responses for all modes of interest.

Modal frequencies between 0 and 25 000 Hz were determined from the transfer function as measured from the blade tip trailing edge (fig. 6). Displacements from numerous accelerometer locations on the blade were processed by the analyzer to determine the mode shapes. The mode shapes for the first three modes were recognized as to whether the blades' motion was bending, torsion, or edgewise. The mode shapes at the higher modes were difficult to classify.

Since the blades are small, adding mass to the blade with both the magnetic chip and accelerometer reduces the modal frequencies. Therefore, holography was used to determine the correct values.

### Holography

Testing was performed in the holographic laboratory at the NASA Lewis Research Center. The blades were indirectly excited by a Piezoelectric Direct Contact Exciter which was located at the mounting block. The Piezoelectric Direct Contact Exciter was able to excite the blade through base excitation without coming in contact with the blades' airfoil section. Speckle interferometry was used to identify natural frequencies by visual inspection of the vibratory modes (fig. 7(a)). The modal frequencies and mode shapes were recorded and photographed.

The results using this procedure were checked against the modal analyzer test results because holography has been known to produce nonexistent or "phantom" modes. Since the blades are highly cambered, holographic mode shape pictures for the edgewise and first torsion mode are similar. The mode shapes from the modal analyzer were used to distinguish the edgewise mode from the first torsion mode.

## ANALYTICAL PROCEDURES

### Finite Element Model

MSC/NASIRAN was used to perform the analysis (ref. 3). The finite element model consisted of 1025 solid eight-node hexahedron elements with 3 degrees of freedom per node (fig. 8).

The base of the blade was fully constrained at the center of the uppermost fir-tree attachment lobe (fig. 2). The in-disk span length was defined from this attachment point to the blade tip. The in-disk span length was assumed to simulate the blades' span length under actual rotor conditions.

A geometric nonlinear, large displacement, static analysis was used to determine the steady state displacements of the blade under centrifugal and thermal loading. Then a normal modes analysis was performed on the updated geometry to estimate the natural frequencies and mode shapes of the blades.

### Material Properties

The single crystal material property specification was obtained from reference 4 by defining an orthotropic material compliance matrix. The generalized stiffness matrix was obtained by inverting the compliance matrix as shown in figure 9. The stiffness coefficients for the SC PWA-1480 and SC MAR-M-247 materials are shown in table II. Since, the elastic properties of SC MAR-M-246 + Hf were unavailable, the properties of MAR-M-247 were used because they are very similar according to NASA Lewis Research Center's Materials Division.

A cylindrical coordinate system was defined to specify the crystal orientation within the blade. The variation in the single crystal orientation was accommodated by supplying the appropriate direction cosines for the material coordinate system. The SC material properties supplied in table II correspond to the crystal properties along the  $\langle 100 \rangle$ ,  $\langle 010 \rangle$ , and  $\langle 001 \rangle$  directions. Young's Modulus was greatest along the crystal's  $\langle 111 \rangle$  direction.

### Loading

The simulation of the SSME turbine blade under actual operating conditions was based on mission profile information obtained from the manufacturer. This information was used to model the centrifugal and thermal loading conditions. Aerodynamic loading conditions were neglected for these analyses. Figure 10 outlines a typical turbopump rotor speed variation during the 8 min launch period. This figure indicates the majority of time spent during pump operation was at either of two distinct rotor speeds (A and B). Times spent at other speeds during pump acceleration/deceleration were considered less significant from a vibration analysis viewpoint.

A temperature-time plot which describes the first stage turbine discharge gas temperature for a typical mission is shown in figure 11. Comparison to figure 10 indicates a sudden change in gas temperature is linked to an instantaneous change in rotor speed. Thus the investigation of either speed A or B from figure 10 will uniquely define a gas temperature from figure 11. The high

heat flux rate under steady-state engine operation results in a very quick blade temperature change between engine speeds. An investigation of the thermal stress dynamics was beyond the intent of this study. The effect of the material softening was considered as of primary importance for the modal analysis "at-speed."

The steady-state operating temperature of the blades at the two speeds was assumed constant throughout the blade airfoil. The temperature distribution was assumed linear through the platform region. The blade shank area was maintained at a constant temperature (900 °F) during the analysis.

## RESULTS

### Model Verification

The experimental modal frequencies for the five tested SC MAR-M-246 + Hf second stage blades are presented in table I. Although the modal frequencies for each blade were different, the holographic mode shapes for all five blades were nearly identical. The mode shapes for blade No. 12238 are shown in figure 7(b). Even though these modes are not pure beam modes, they can be classified using beam terminology. Mode 1 proved to be first bending in the flatwise direction. Modes 2 and 3 were difficult to distinguish. The two modes appear the same because of the blades' high camber. Data from the FFT method indicated mode 2 to be first torsion and mode 3 to be bending in the edgewise direction. Mode 4 was second bending. At the higher modes, mode 5 appeared to be the lyre mode and mode 6 (not shown) was a tip mode.

These experimental results, modal frequencies and mode shapes, were compared with results from a finite element model of similar material and crystal orientations. These results were used to verify and determine the accuracy of the finite element model for the second stage blade.

The finite element analysis results are presented in table I. The analytical results from blade No. 12238 had excellent agreement with the holographic results (figs. 7(a) and (b)). The first five mode shapes duplicated the holograms. Comparisons between the first four frequency results indicates the finite element model was slightly stiffer than the experimental cases.

Efforts were focused upon the possible softening effects of the braze material between the mounting block and blade. Attempts were made to model the braze material at this interface. The braze material had no effect on the modal frequencies of the blade as shown in table III.

The frequency was found to be very sensitive to blade span length. A 2 percent increase in span length decreased some frequencies by up to 11 percent (table IV). Each tested blade was measured to determine its tested span length. The in-block span length was measured from the blade tip to the top of the braze where the fir tree is fixed. The in-block span length was slightly longer than the in-disk span length. The analytical results of the second stage blades compared very well with the experimental results when using the in-block span length as shown in table I.

The subsequent analyses on the first stage blades using PWA-1480 material were performed for an in-disk condition at a blade span length of 1.34 in. as determined from the Engineering Drawings and Specifications (ref. 2). It was determined that this span length would best simulate the blade under actual rotor conditions. The blade was fixed at its upper most lobe on the fir tree (fig. 2).

The SC first stage blades are easily manufactured with their crystal growth direction aligned in the blades' span direction, similar to the DS blades. The SC blades supplied for the bench tests had tilt angles within  $10^\circ$  of  $54.74^\circ$ . Therefore, a tolerance of  $\pm 10^\circ$  was applied to the tilt angle. The analyses were performed for the following tilt angles:  $44.74^\circ$ ,  $54.74^\circ$ , and  $64.74^\circ$ .

### Parametric Study

A parametric study was performed on the SSME First Stage HPFTP blades investigating the effect of crystal orientation on the blades natural frequencies. Figures 12 to 29 graphically represent frequency, as a function of rotation angle for three distinct tilt angles. The effects of orientations on the first six blade modes using SC PWA-1480 material are shown. The analyses using SC PWA-1480 material were conducted at both nonrotating room temperature conditions and operating conditions. Results of the parametric study are as follows:

(1) The general trends of the modal frequencies as a function of crystal orientation for nonrotating and rotating conditions are the same at each mode. The frequencies at a tilt angle of  $54.74^\circ$  are periodic for every  $90^\circ$  of rotation.

(2) For the first three modes the tilt angle has a slightly greater influence on the modal frequencies. But this effect is small, i.e. less than 5 percent change in frequency for  $\pm 10^\circ$  change in tilt angle.

(3) For the higher modes, four through six, the orientation angle influence is reversed. There are larger variations in frequency due to rotation angle rather than tilt angles. Again, the percent change in frequency is small.

(4) Comparisons of the frequencies at two different pump speeds, 27 500 and 36 000 rpm, were very similar. The thermal softening effects dominate the centrifugal stiffening effects. The temperature distributions during pump operation caused a significant softening effect on the blade's structural stiffness.

### Campbell Diagrams

The Campbell Diagrams for the SC PWA-1480 blades were constructed. Considerations were given within the diagrams to a  $\pm 5$  percent deviation in excitation frequency. Critical engine orders were based on the following upstream conditions as determined from Rocketdyne (ref. 5);

(1) Engine order 11, 13, 15, 24, 26, and 28 - These engine orders are based on the 13 upstream struts. Six struts are located at  $180^\circ$  within the diameter while seven struts are at the remaining  $180^\circ$ . The struts are not equally spaced.

(2) Engine order 41 - This engine order is based on the 41 equally spaced upstream nozzles.

Campbell Diagrams at nominal orientations (spanwise material solidification direction) for the SC PWA-1480 blade (tilt =  $54.74^\circ$ , rotate =  $0.0^\circ$ ) were compared against the DS MAR-M-246 + Hf blade. Critical crossings for the DS blade are at the first mode - 11th engine order - 27 500 RPM, second mode - 24th engine order - 27 500 RPM, third mode - 24th engine order - 35 000 RPM, and the fourth mode - 28th engine order - 35 000 RPM (fig. 30). Whereas, critical crossings for the SC blade are at the first mode - 11th engine order - 27 500 RPM, at the second mode - 24th engine order - 27 500 RPM, and at the third mode - 24th engine order - 35 000 RPM (fig. 31).

From a dynamics viewpoint the SC blade appears to be a slight improvement over the DS blade since one engine order interference was eliminated at the fourth mode. The encouraging aspect at this point is that no new engine order interferences were introduced with the material substitution.

The critical engine order excitations can be reduced by reorienting the crystal within the tolerance limits of the  $54.74^\circ$  tilt angle. Critical engine order excitations may occur at two locations when the crystal was oriented at a tilt angle of  $64.74^\circ$  and rotate angle of  $60.0^\circ$ . Figure 32 shows that these crossings may occur at the first mode - 11th engine order - 27 500 RPM and at the third mode - 24th engine order - 35 000 RPM. The second mode falls between the 24th and 26th engine order at 27 500 RPM. Excitation could occur at this mode depending on the variations in pump speed.

Possible critical engine order excitations are occurring within the blades' first three modes under operating conditions at nominal orientations. Previous analyses had shown that these modes were primarily influenced by variations in the crystal tilt angle. The crystal  $\langle 111 \rangle$  axis orientation was varied between the extremes of spanwise to chordwise. Figures 33 to 44 show the blades modal frequency variations with respect to tilt angle. Aligning the crystal's stiff axis within the blades spanwise direction (tilt =  $0^\circ$ ) increases the first modal frequency (bending mode) and decreases the second modal frequency (torsion mode). The opposite was true when aligning the crystal's stiff axis within the blades chordwise direction (tilt =  $90^\circ$ ).

Common practice in analyzing Campbell Diagrams is to apply a  $\pm 5$  percent deviation in excitation frequency at the first mode. This deviation decreases at the upper modes. Therefore, a  $\pm 5$  percent deviation in rotor speed and excitation frequency was conservatively applied to all the engine orders and to all the natural responses of the SC blade respectfully. This tolerance would account for any variations in rotor speed and blade-to-blade differences due to manufacturing.

Attempts were made to find an orientation which would eliminate or minimize the critical engine order excitations. Figure 45 shows that orienting the 111 axis in the spanwise direction effects the first and third mode between several critical engine orders. Whereas, figures 46 and 47 show that orienting

the  $\langle 111 \rangle$  axis in the chordwise direction can be beneficial. The number of critical excitations were reduced when compared to the DS blade and the SC nominal orientation as shown in table V. However, for any SC orientation the third mode interference will exist when considering a  $\pm 5$  percent deviation of excitation frequency (fig. 41).

## SUMMARY AND CONCLUSIONS

A summary of the conclusions developed from the analysis and tests are as follows;

1. From a dynamics viewpoint, the SC blade is an improvement over the DS blade. No new engine order interferences were introduced with the PWA-1480 material substitution. The SC blade at the nominal orientation was found to be better than the DS blade because the fourth mode interference was eliminated. However, interferences still exist at modes 1 to 3.

2. The engine order interferences within the SC blades first three modes can be minimized by changing the crystal orientation. The best orientation is to align the crystals' 111 axis in the blades' chord direction or at a tilt angle of  $90^\circ$ . However, it was found that for any orientation, the third mode interference will exist.

3. The blade natural frequencies are very sensitive to support location. Extreme care is needed both experimentally and analytically in simulating disc support conditions.

4. For the first three modes the tilt angle has a slightly greater influence on the modal frequencies than rotate angle. But this effect is small, i.e., less than 5 percent change in frequency for  $\pm 10^\circ$  change in tilt angle.

5. The procedure of using a  $\pm 5$  percent tolerance of excitation frequency in the Campbell Diagrams may be conservative. The actual blade-to-blade differences in natural frequencies due to the manufacturing processes should be determined by testing a large sample of SC blades at similar orientations.

6. This preliminary investigation was a limited scope study. A more detailed study with respect to thermal, mechanical, and orientation effects is recommended.

## ACKNOWLEDGMENTS

This report is based on work supported by NASA Lewis Research Center under Contract NAS3-24105. The authors wish to thank Dr. Robert E. Kielb and Dr. Robert L. Dreshfield for their assistance.

## REFERENCES

1. Dreshfield, R.L.; and Parr, R.A.: Application of Single Crystal Superalloys for Earth-to-Orbit Propulsion Systems. AIAA Paper 87-1976, June 1987. (NASA TM-89877).

2. Engineering Drawings and Specifications for the Single Crystal First Stage Turbine Blades in the SSME HPFTP, supplied by Rockwell International, Rocketdyne Division, Canoga Park, CA.
  - a. RS007502 Rocket Engine High Pressure Fuel Turbopump Assembly
  - b. RS018581 First Stage Rotor High Pressure Fuel Turbopump Blade
  - c. RS007517 First Stage Rotor High Pressure Fuel Turbopump Disk
  - d. RL00351 High Pressure Fuel Turbopump Assemble and Checkout Specification
  - e. RL00352 SSME High Pressure Fuel Pump Rotor Dynamic Balance Specification
3. Joseph, J.A., ed.: MSC/NASTRAN Application Manual. MacNeal-Schwendler, 1981.
4. Bowen, K.; Nagy, P.; and Parr, R.A.: The Evaluation of Single Crystal Superalloys for Turbopump Blades in the SSME. AIAA Paper 86-1477, June 1986.
5. Davis, G.: Personal Communication. Rockwell International, Rocketdyne Division, Canoga Park, CA.

TABLE I. - MODAL FREQUENCY COMPARISON BETWEEN HOLOGRAPHY AND MSC/NASTRAN SSME HPFTP SECOND-STAGE BLADE

[H = Holography frequencies (Hz), N = NASTRAN frequencies (Hz),  
... and P = percent difference =  $[(N - H)/H] \times 100$  percent.]

Blade ID	12238			09382			11826			12354			12436		
Orientation Tilt, degree	50.4			54.4			59.0			48.6			47.3		
Rotate, degree	48.8			63.9			43.7			89.8			9.5		
Mode	H	N	P	H	N	P	H	N	P	H	N	P	H	N	P
1	4 632	4 634	+0.4	4 651	4 785	+2.9	4 599	4 737	+3.0	4 742	4 722	-.42	4 656	4 743	+1.9
2	9 989	10 251	+2.6	9 879	10 498	+6.2	9 850	10 559	+7.2	9 989	10 049	+6.0	9 719	9 717	-.02
3	13 011	13 805	+6.1	12 820	13 992	+9.1	13 529	13 883	+2.6	13 011	13 922	+7.0	12 830	13 474	+5.0
4	16 472	16 447	-.15	16 473	16 903	+2.6	16 817	16 786	-.18	16 472	16 501	+1.7	16 249	16 315	+4
5	19 611	20 159	+2.8	19 293	20 568	+6.6	20 817	20 490	-1.6	19 611	19 120	-2.5	21 936	18 876	-14.0
6	22 417	21 420	-4.4	20 157	21 977	+2.0	20 856	21 695	+4.0	22 417	21 194	-5.5	22 045	21 092	-4.3

TABLE II. - SINGLE CRYSTAL MATERIAL  
STIFFNESS COEFFICIENTS AS A  
FUNCTION OF TEMPERATURE

Temperature, F	Stiffness coefficients		
	C11 MPSI	C12 MPSI	C44 MPSI
MAR-M-247 Material			
70	39.3	26.2	18.6
PWA-1480 Material			
70	35.5	23.0	18.0
200	35.5	23.0	18.0
400	35.0	23.0	17.5
600	34.6	22.7	17.0
800	34.2	22.5	16.5
1000	33.7	22.3	16.0
1200	33.2	22.1	15.5
1400	32.5	22.0	15.0
1600	31.5	21.8	14.5
1800	30.5	21.7	14.0

TABLE III. - EFFECTS OF BRAZE MATERIAL  
ON THE MODAL FREQUENCIES OF  
SC SSME HPFTP BLADE MODEL

Mode	Modal frequencies, Hz	
	Modeled with braze material	Modeled without braze material
1	4 735	4 735
2	11 818	11 819
3	14 737	14 739
4	17 546	17 547
5	21 503	21 503
6	24 913	24 914

TABLE IV. - SPAN LENGTH EFFECTS ON MODAL  
FREQUENCIES OF SC SSME HPFTP  
BLADE MODEL

Mode	Modal frequencies, Hz		
	Span length, 1.3219 in.	Span length, 1.3432 in.	Percent change
1	5 313	5 129	-3.5
2	12 156	10 839	-10.8
3	16 032	14 818	-7.6
4	19 392	17 552	-9.5
5	23 140	21 098	-8.8

TABLE V. - ENGINE ORDER INTERFERENCES

Mode	Directionally solidified material	Single crystal material tilt = 54.74 rotate = 0.0	SC optimum orientation tilt = 90.0 rotate = 0.0
1	11E	11E	11E to 13E
2	24E	24E	None
3	24E	24E	24E to 26E
4	28E	None	None
5	None	None	None
6	None	None	None

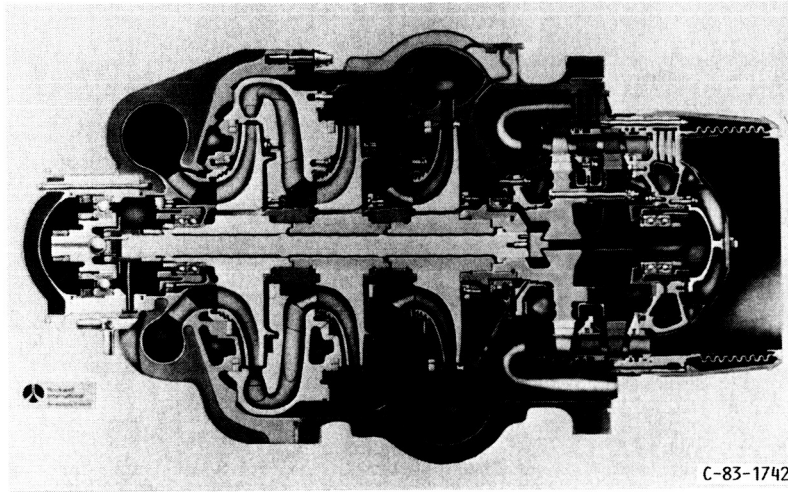


FIGURE 1. - SSME HIGH PRESSURE FUEL TURBOPUMP (HPFTP).

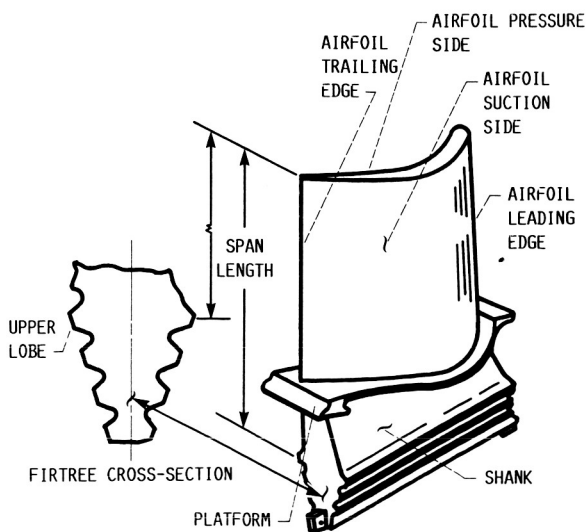
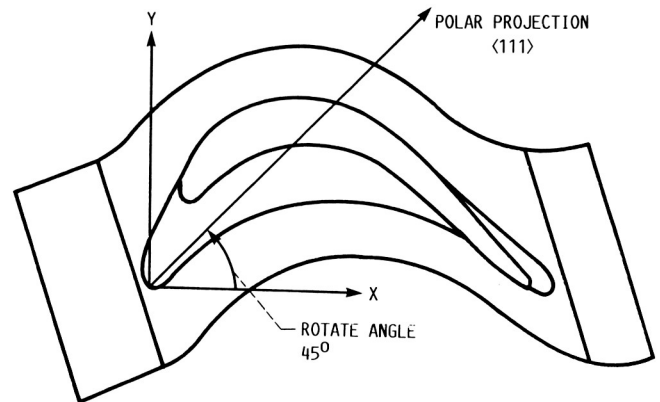


FIGURE 2. - SSME HPFTP FIRST-STAGE TURBINE BLADE.

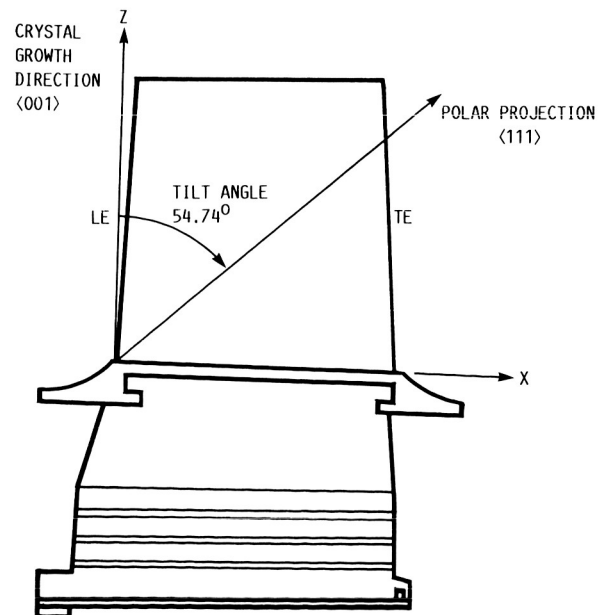


FIGURE 3. - MATERIAL ORIENTATION OF SINGLE-CRYSTAL BLADE.

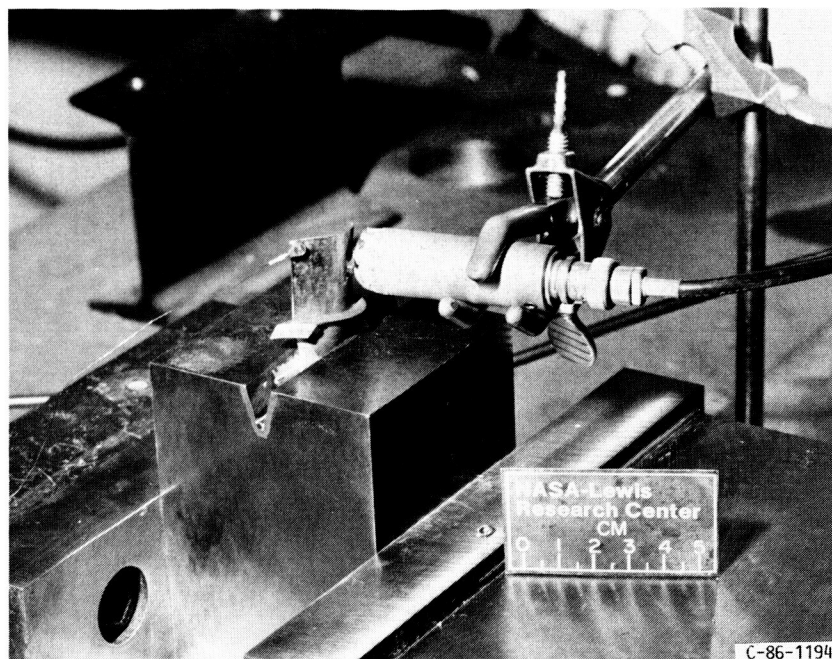


FIGURE 4. - MODAL ANALYZER EXPERIMENTAL APPARATUS.

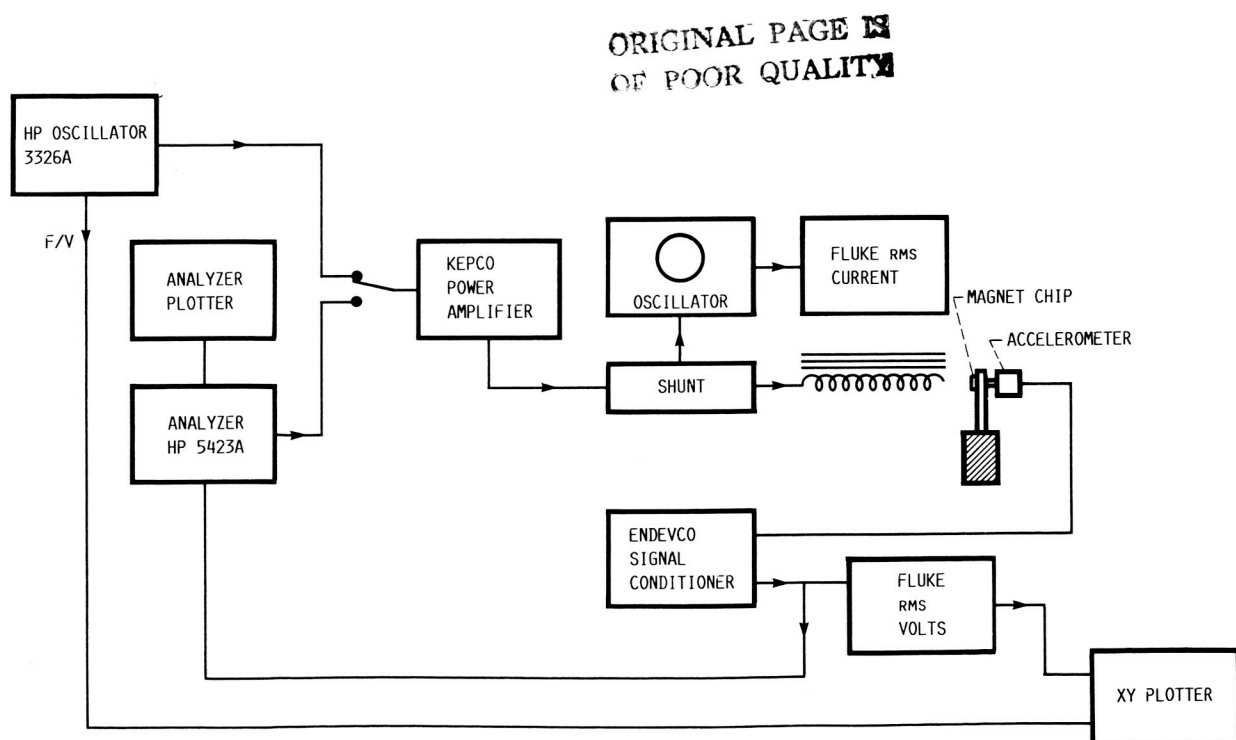


FIGURE 5. - MODAL ANALYZER EXPERIMENTAL SCHEMATIC.

ORIGINAL PAGE IS  
OF POOR QUALITY

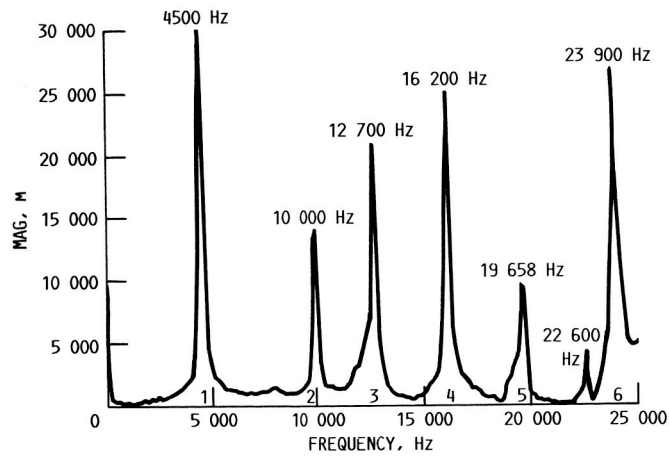
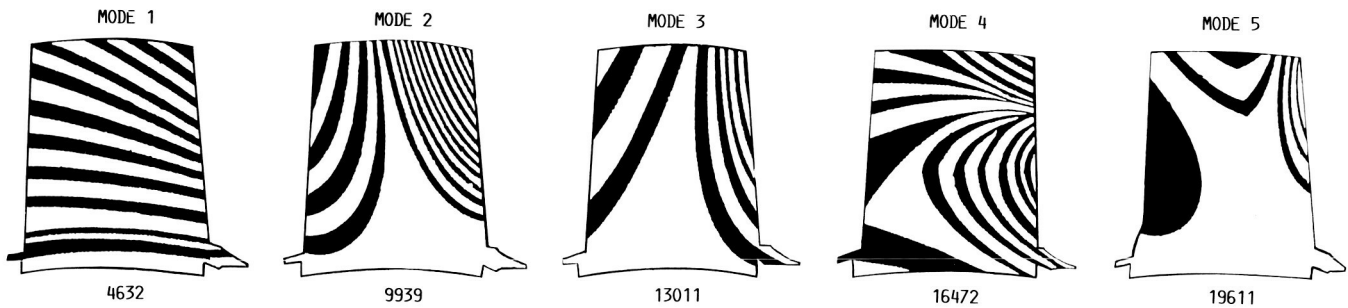
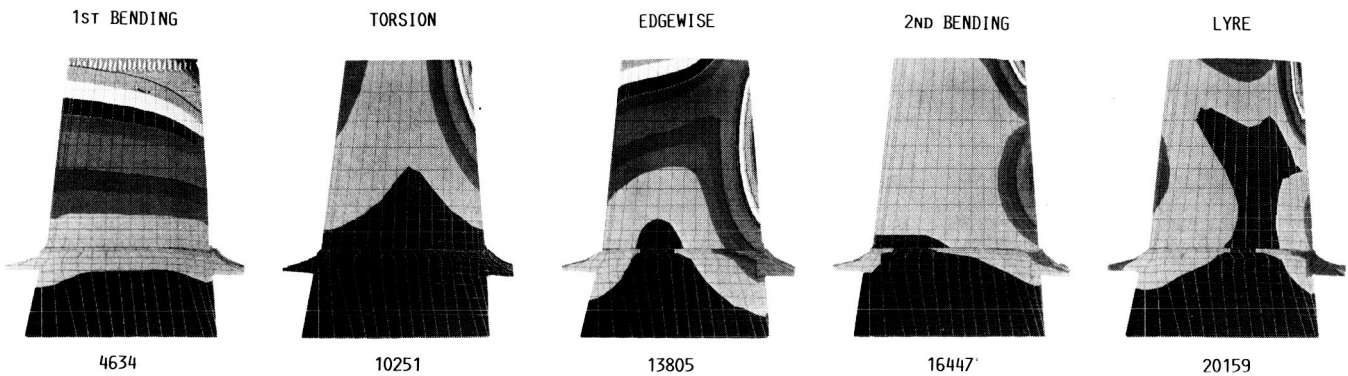


FIGURE 6. - AUTO SPECTRA DATA.



(A) HOLOGRAPHIC FREQUENCIES/MODE SHAPES.



(B) MSC/NASTRAN FREQUENCIES/MODE SHAPES.

FIGURE 7. - SSME HPFTP SECOND-STAGE BLADE.

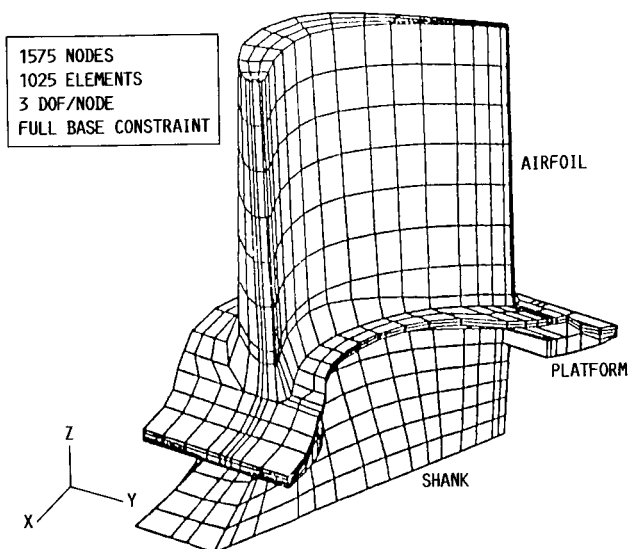


FIGURE 8. MSC/NASTRAN FINITE ELEMENT MODEL.

AN ORTHOTROPIC MATERIAL STIFFNESS MATRIX IS DEFINED AS:

$$[C] = \begin{bmatrix} C_{11} & C_{12} & C_{13} & 0 & 0 & 0 \\ C_{12} & C_{22} & C_{23} & 0 & 0 & 0 \\ C_{13} & C_{23} & C_{33} & 0 & 0 & 0 \\ 0 & 0 & 0 & C_{44} & 0 & 0 \\ 0 & 0 & 0 & 0 & C_{55} & 0 \\ 0 & 0 & 0 & 0 & 0 & C_{66} \end{bmatrix}$$

FOR THE ANISOTROPIC SINGLE CRYSTAL, THE INDEPENDENT STIFFNESS COEFFICIENTS ARE RELATED TO THE COMPLIANCE MATRIX [S] AS:

$$C_{11} = \frac{S_{11} + S_{12}}{(S_{11} - S_{12})(S_{11} + 2S_{12})}$$

$$C_{12} = \frac{-S_{12}}{(S_{11} - S_{12})(S_{11} + 2S_{12})}$$

$$C_{44} = \frac{1}{S_{44}}$$

BY SYMMETRY:

$$C_{11} = C_{22} = C_{33}$$

$$C_{44} = C_{55} = C_{66}$$

$$C_{12} = C_{23} = C_{13}$$

FIGURE 9. - SINGLE-CRYSTAL MATERIAL MATRIX FORMULATION.

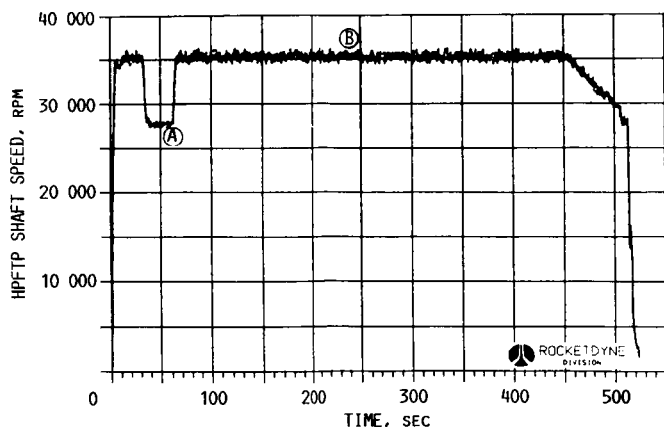


FIGURE 10. - PUMP FLIGHT DATA; HPFTP SHAFT SPEED. (SEE REF. 5.)

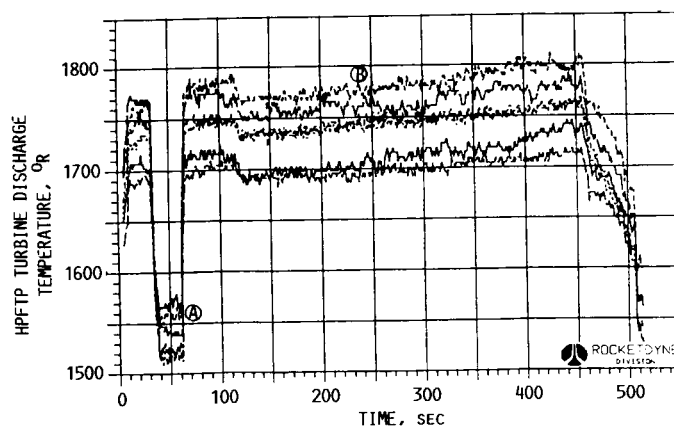


FIGURE 11. - PUMP FLIGHT DATA; HPFTP TURBINE DISCHARGE TEMPERATURE. (SEE REF. 5.)

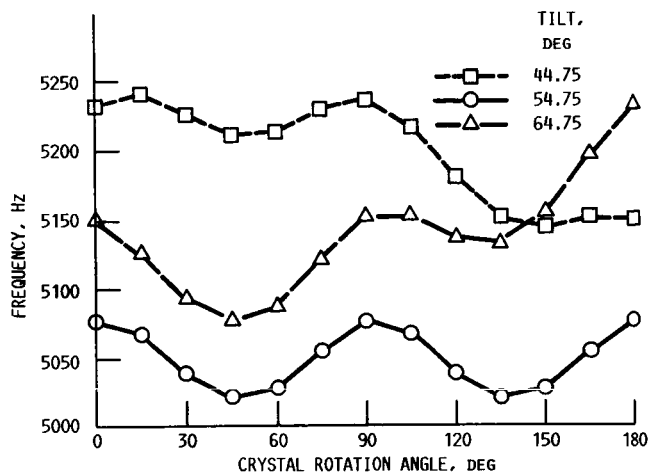


FIGURE 12. - SSME HPFTP FIRST-STAGE BLADE; PWA-1480; NONROTATING; 70 °F; FIRST MODE.

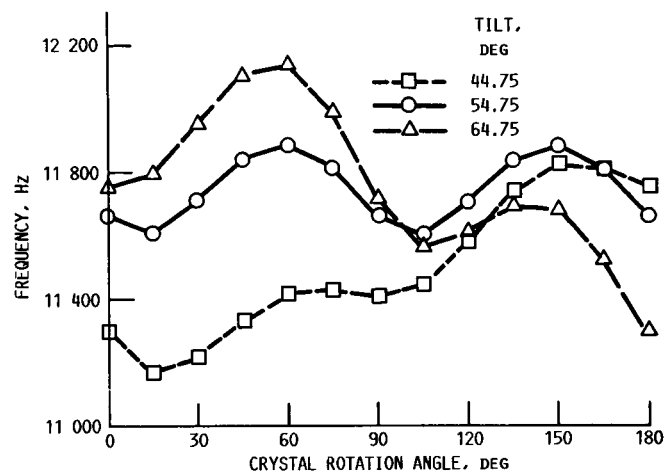


FIGURE 13. - SSME HPFTP FIRST-STAGE BLADE; PWA-1480; NONROTATING; 70 °F; SECOND MODE.

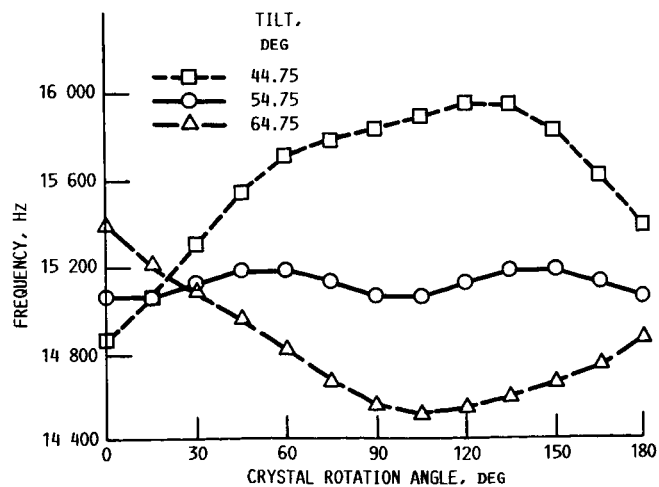


FIGURE 14. - SSME HPFTP FIRST-STAGE BLADE; PWA-1480; NONROTATING; 70 °F; THIRD MODE.

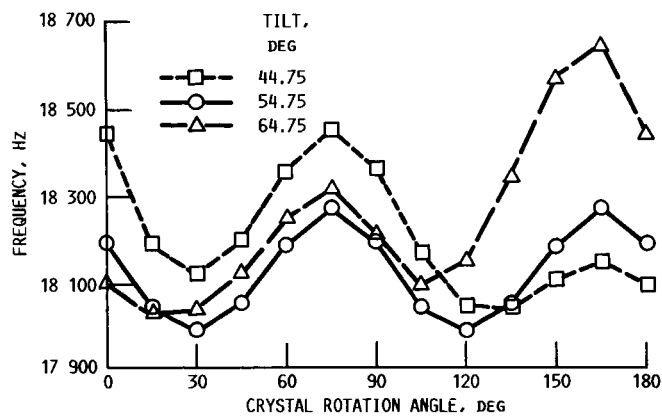


FIGURE 15. - SSME HPFTP FIRST-STAGE BLADE; PWA-1480; NONROTATING; 70 °F; FOURTH MODE.

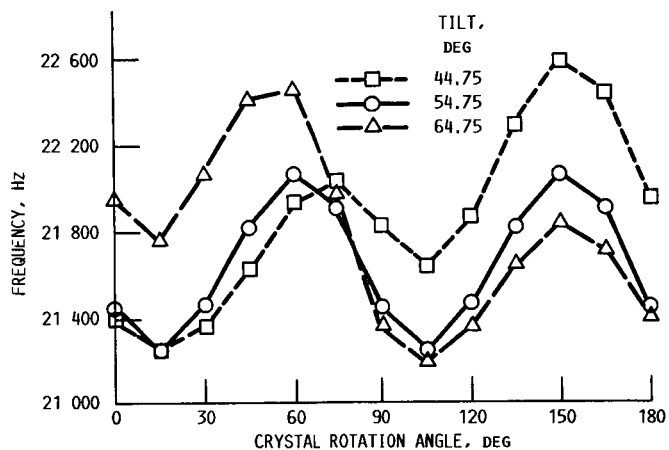


FIGURE 16. - SSME HPFTP FIRST-STAGE BLADE; PWA-1480; NONROTATING; 70 °F; FIFTH MODE.

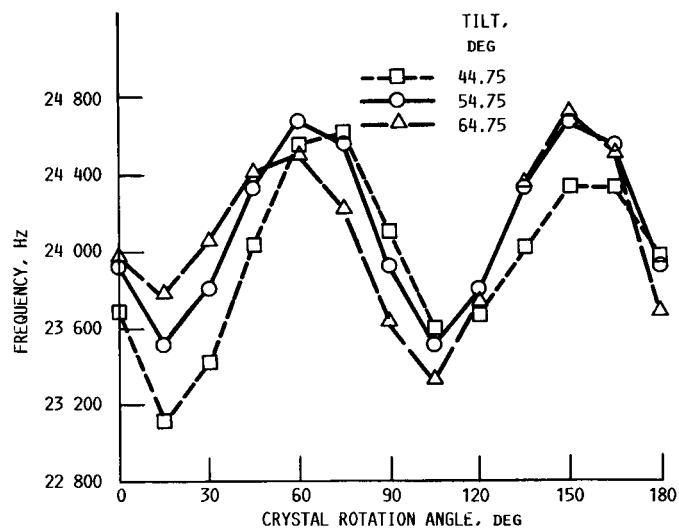


FIGURE 17. - SSME HPFTP FIRST-STAGE BLADE; PWA-1480; NONROTATING; 70 °F; SIXTH MODE.

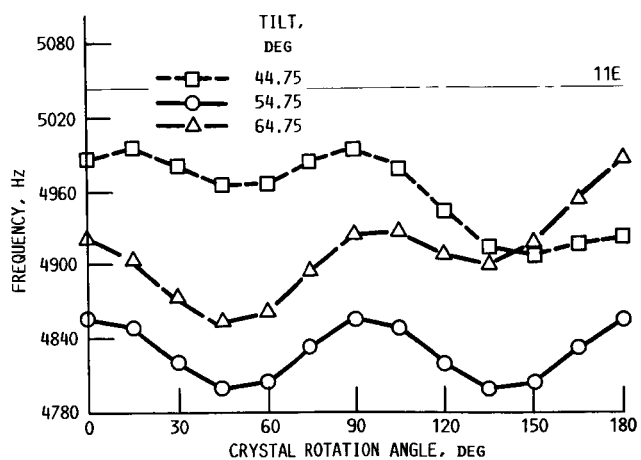


FIGURE 18. - SSME HPFTP FIRST-STAGE BLADE; PWA-1480; 27 500 RPM;  $T_{af} = 1200$  °F AND  $T_{sh} = 1000$  °F; FIRST MODE. (NOTE:  $T_{af}$  = STEADY STATE TEMPERATURE AIR-FOIL AND  $T_{sh}$  = STEADY STATE TEMPERATURE SHANK.)

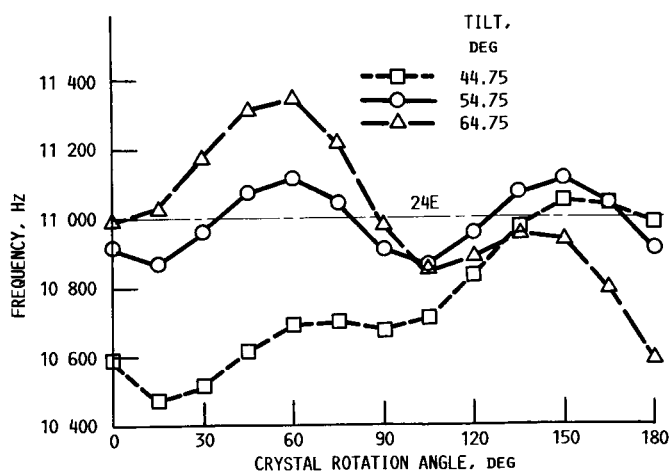


FIGURE 19. - SSME HPFTP FIRST-STAGE BLADE; PWA-1480; 27 500 RPM;  $T_{af} = 1200$  °F AND  $T_{sh} = 1000$  °F; SECOND MODE.

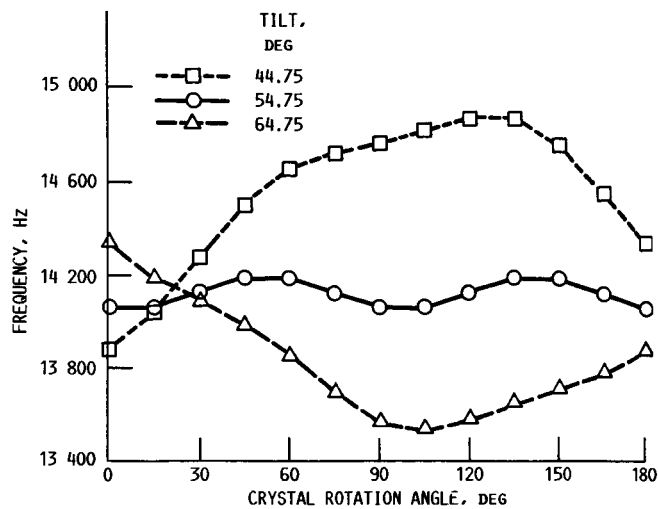


FIGURE 20. - SSME HPFTP FIRST-STAGE BLADE; PWA-1480; 27 500 RPM;  $T_{af} = 1200^{\circ}\text{F}$  AND  $T_{sh} = 1000^{\circ}\text{F}$ ; THIRD MODE.

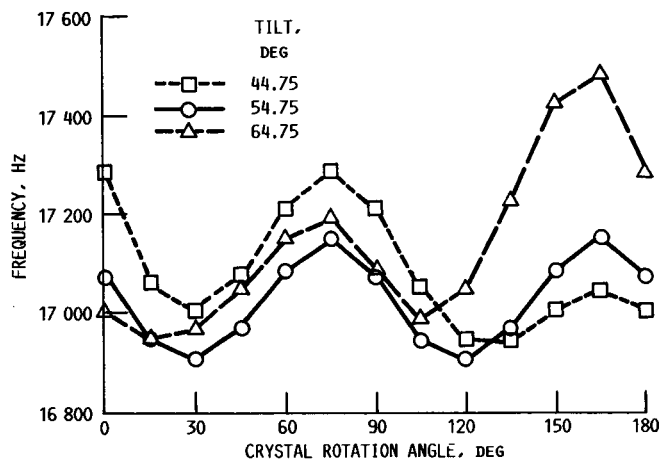


FIGURE 21. - SSME HPFTP FIRST-STAGE BLADE; PWA-1480; 27 500 RPM;  $T_{af} = 1200^{\circ}\text{F}$  AND  $T_{sh} = 1000^{\circ}\text{F}$ ; FOURTH MODE.

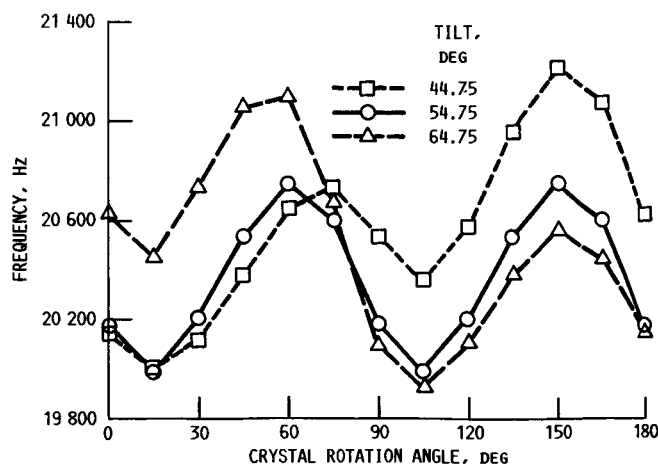


FIGURE 22. - SSME HPFTP FIRST-STAGE BLADE; PWA-1480; 27 500 RPM;  $T_{af} = 1200^{\circ}\text{F}$  AND  $T_{sh} = 1000^{\circ}\text{F}$ ; FIFTH MODE.

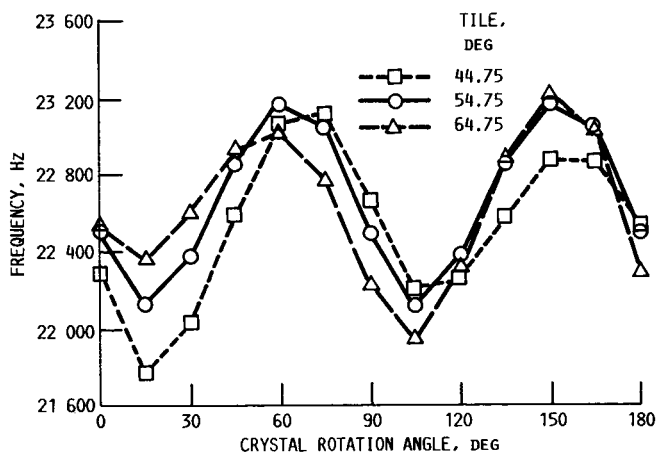


FIGURE 23. - SSME HPFTP FIRST-STAGE BLADE; PWA-1480; 27 500 RPM;  $T_{af} = 1200^{\circ}\text{F}$  AND  $T_{sh} = 1000^{\circ}\text{F}$ ; SIXTH MODE.

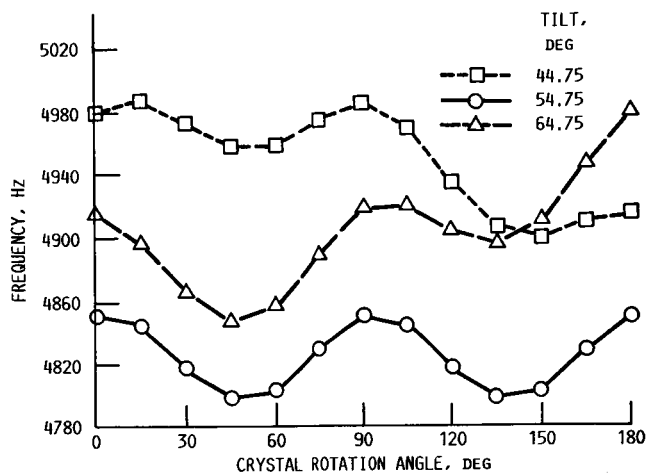


FIGURE 24. - SSME HPFTP FIRST-STAGE BLADE; PWA-1480; 35 000 RPM;  $T_{af} = 1400^{\circ}\text{F}$  AND  $T_{sh} = 1200^{\circ}\text{F}$ ; FIRST MODE.

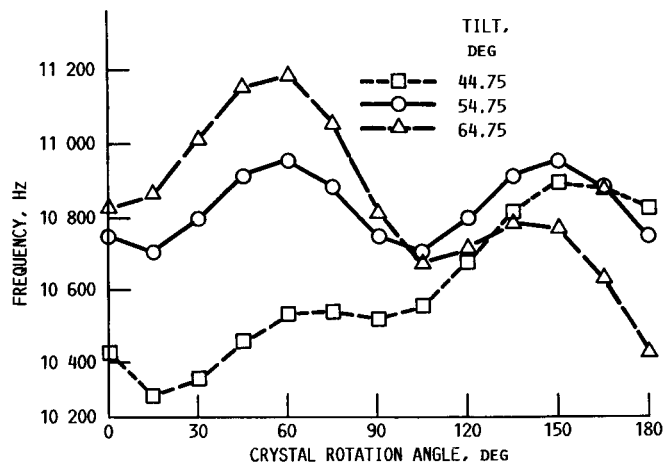


FIGURE 25. - SSME HPFTP FIRST-STAGE BLADE; PWA-1480; 35 000 RPM;  $T_{af} = 1400^{\circ}\text{F}$  AND  $T_{sh} = 1200^{\circ}\text{F}$ ; SECOND MODE.

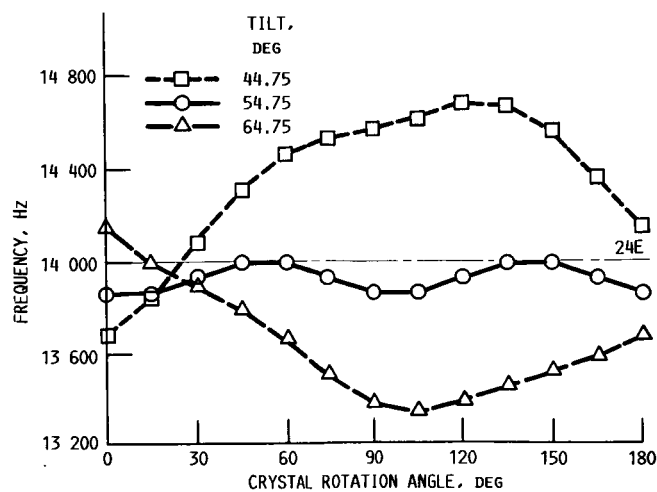


FIGURE 26. - SSME HPFTP FIRST-STAGE BLADE; PWA-1480; 35 000 RPM;  $T_{af} = 1400^{\circ}\text{F}$  AND  $T_{sh} = 1200^{\circ}\text{F}$ ; THIRD MODE.

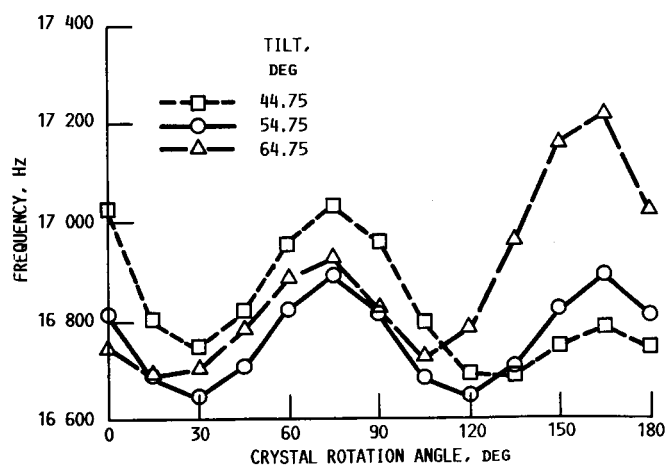


FIGURE 27. - SSME HPFTP FIRST-STAGE BLADE; PWA-1480; 35 000 RPM;  $T_{af} = 1400^{\circ}\text{F}$  AND  $T_{sh} = 1200^{\circ}\text{F}$ ; FOURTH MODE.

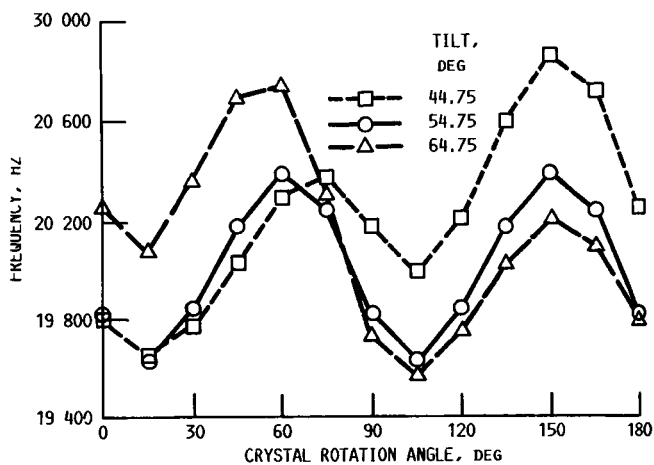


FIGURE 28. - SSME HPFTP FIRST-STAGE BLADE; PWA-1480; 35 000 RPM;  $T_{af} = 1400^{\circ}\text{F}$  AND  $T_{sh} = 1200^{\circ}\text{F}$ ; FIFTH MODE.

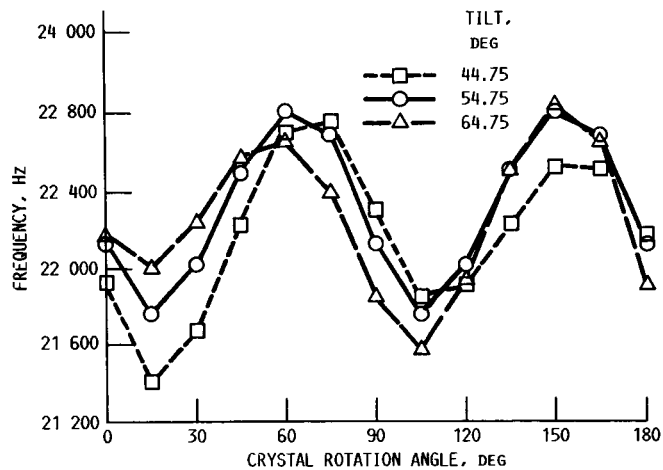


FIGURE 29. - SSME HPFTP FIRST-STAGE BLADE; PWA-1480; 35 000 RPM;  $T_{af} = 1400^{\circ}\text{F}$  AND  $T_{sh} = 1200^{\circ}\text{F}$ ; SIXTH MODE.

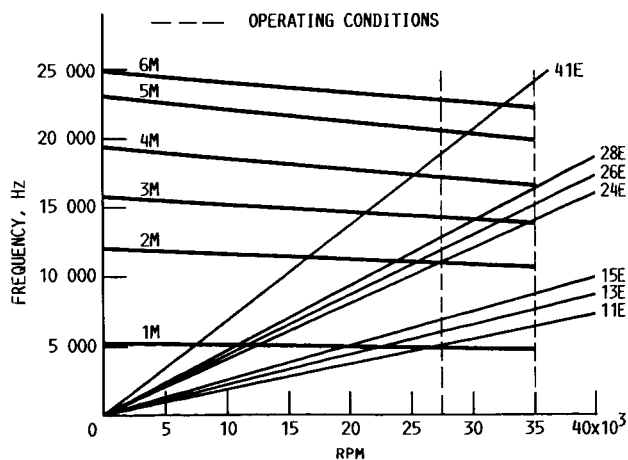


FIGURE 30. - SSME HPFTP FIRST-STAGE BLADE; CAMPBELL DIAGRAM; DS MAR-M-246 Hf MATERIAL.

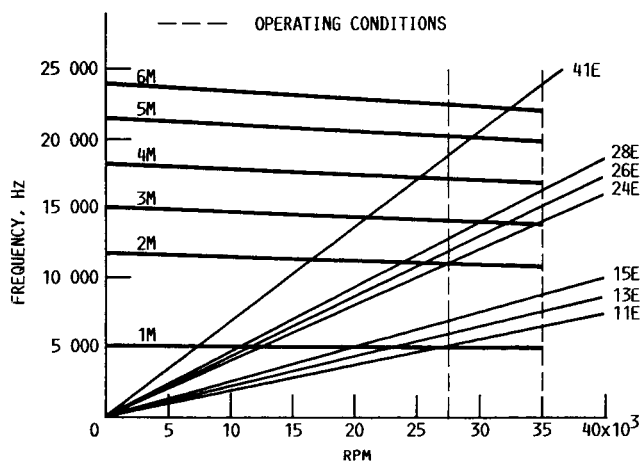


FIGURE 31. - SSME HPFTP FIRST-STAGE BLADE; CAMPBELL DIAGRAM; PWA-1480; SC ORIENTATION: TILT =  $54.74^{\circ}$  AND ROTATE =  $0^{\circ}$ .

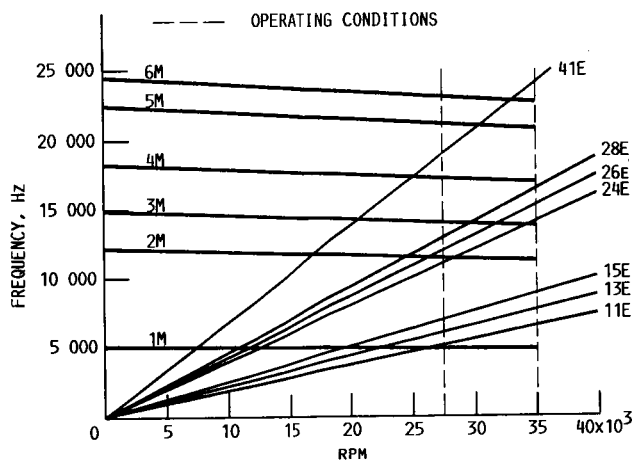


FIGURE 32. - SSME HPFTP FIRST-STAGE BLADE; CAMPBELL DIAGRAM; PWA-1480; SC ORIENTATION: TILT =  $64.74^\circ$  AND ROTATE =  $60^\circ$ .

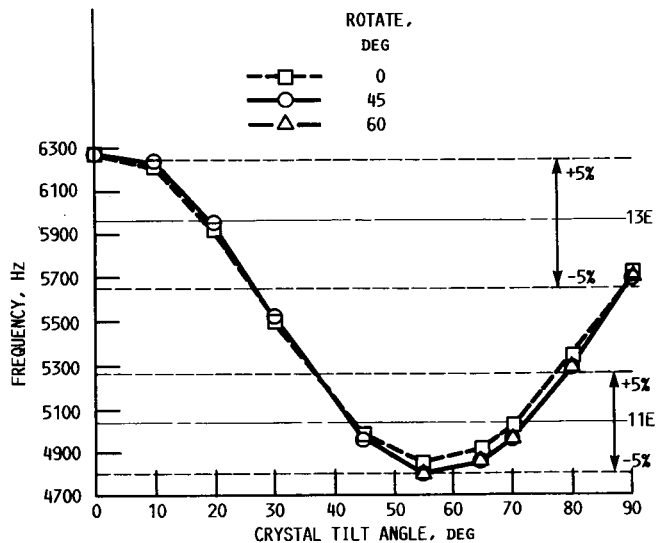


FIGURE 33. - SSME HPFTP FIRST-STAGE BLADE; PWA-1480; 27 500 RPM;  $T_{af} = 1200^\circ\text{F}$  AND  $T_{sh} = 1000^\circ\text{F}$ ; FIRST MODE.

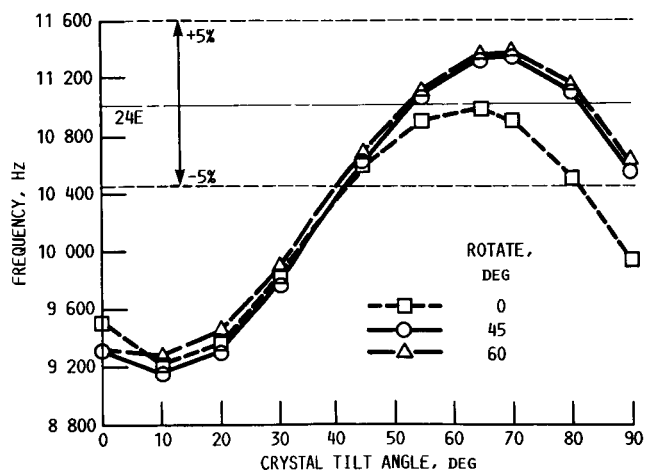


FIGURE 34. - SSME HPFTP FIRST-STAGE BLADE; PWA-1480; 27 500 RPM;  $T_{af} = 1200^\circ\text{F}$  AND  $T_{sh} = 1000^\circ\text{F}$ ; SECOND MODE.

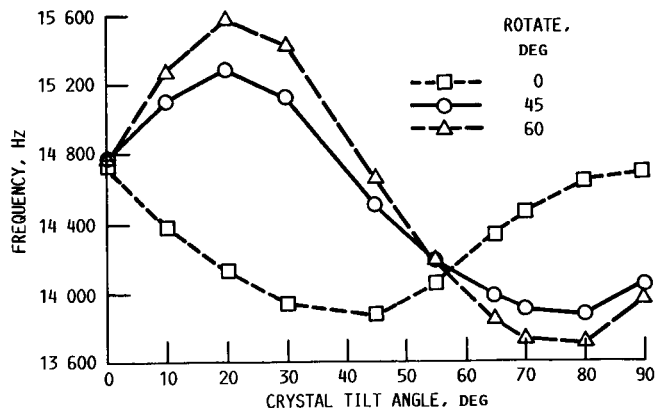


FIGURE 35. - SSME HPFTP FIRST-STAGE BLADE; PWA-1480; 27 500 RPM;  $T_{af} = 1200^\circ\text{F}$  AND  $T_{sh} = 1000^\circ\text{F}$ ; THIRD MODE.

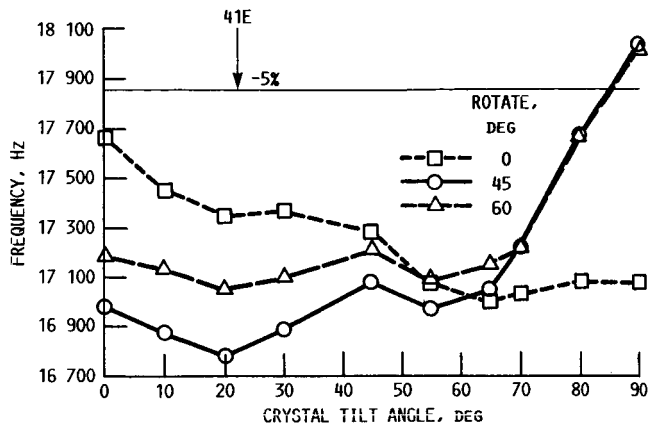


FIGURE 36. - SSME HPFTP FIRST-STAGE BLADE; PWA-1480; 27 500 RPM;  $T_{af} = 1200^{\circ}\text{F}$  AND  $T_{sh} = 1000^{\circ}\text{F}$ ; FOURTH MODE.

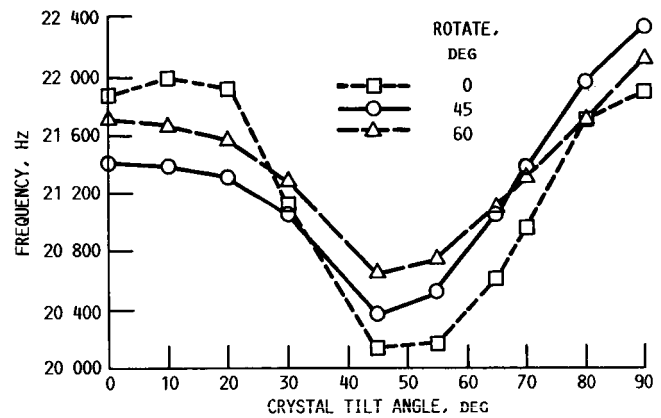


FIGURE 37. - SSME HPFTP FIRST-STAGE BLADE; PWA-1380; 27 500 RPM;  $T_{af} = 1200^{\circ}\text{F}$  AND  $T_{sh} = 1000^{\circ}\text{F}$ ; FIFTH MODE.

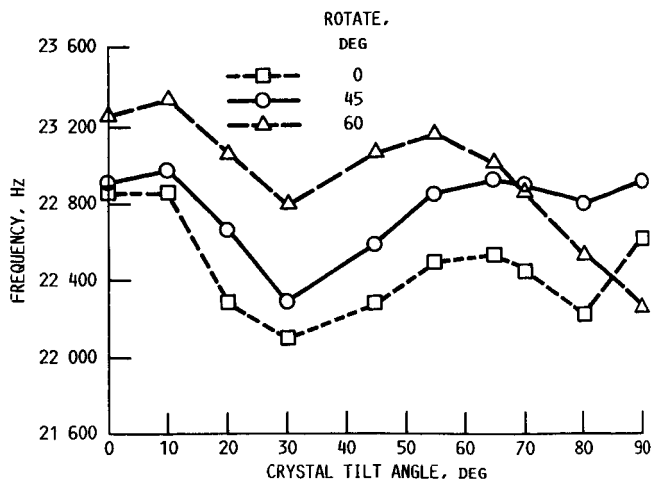


FIGURE 38. - SSME HPFTP FIRST-STAGE BLADE; PWA-1480; 27 500 RPM;  $T_{af} = 1200^{\circ}\text{F}$  AND  $T_{sh} = 1000^{\circ}\text{F}$ ; SIXTH MODE.

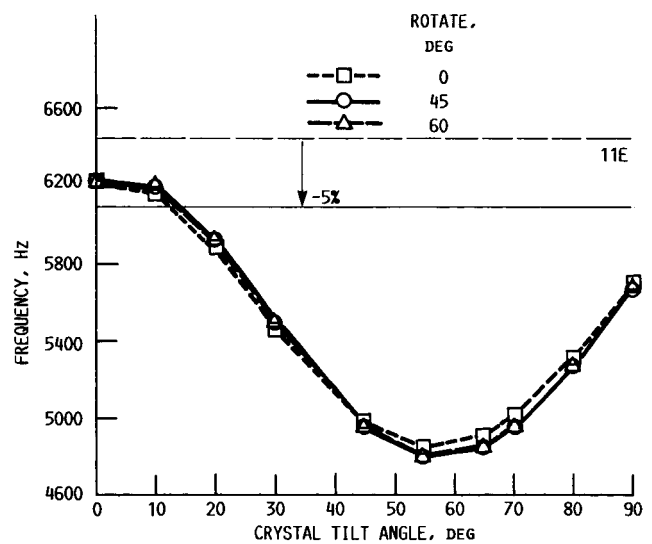


FIGURE 39. - SSME HPFTP FIRST-STAGE BLADE; PWA-1480; 35 000 RPM;  $T_{af} = 1400^{\circ}\text{F}$  AND  $T_{sh} = 1200^{\circ}\text{F}$ ; FIRST MODE.

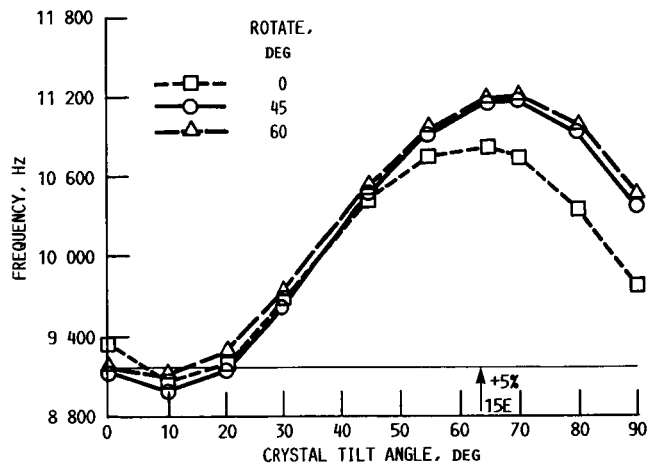


FIGURE 40. - SSME HPFTP FIRST-STAGE BLADE; PWA-1480; 35 000 RPM;  $T_{af} = 1400^{\circ}\text{F}$  AND  $T_{sh} = 1200^{\circ}\text{F}$ ; SECOND MODE.

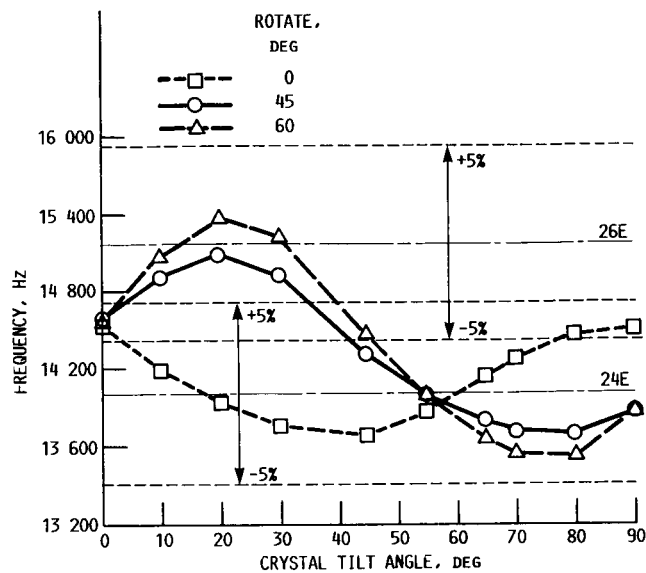


FIGURE 41. - SSME HPFTP FIRST-STAGE BLADE; PWA-1480; 35 000 RPM;  $T_{af} = 1400^{\circ}\text{F}$  AND  $T_{sh} = 1200^{\circ}\text{F}$ ; THIRD MODE.

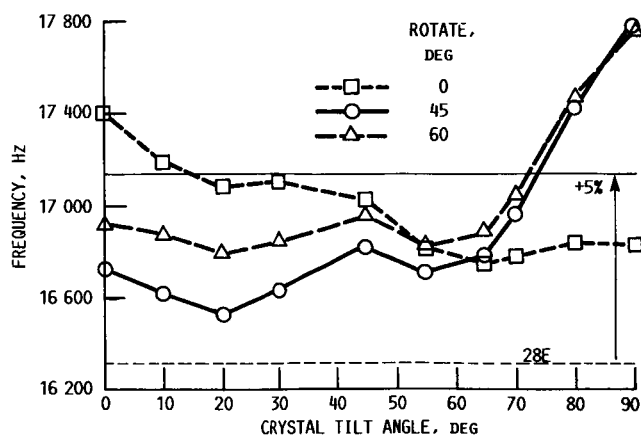


FIGURE 42. - SSME HPFTP FIRST-STAGE BLADE; PWA-1480; 35 000 RPM;  $T_{af} = 1400^{\circ}\text{F}$  AND  $T_{sh} = 1200^{\circ}\text{F}$ ; FOURTH MODE.

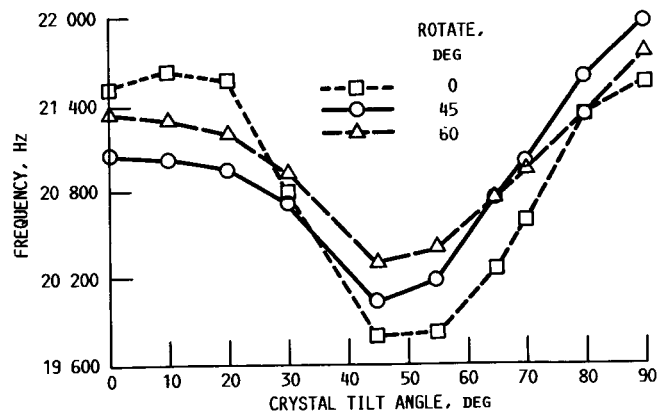


FIGURE 43. - SSME HPFTP FIRST-STAGE BLADE; PWA-1480; 35 000 RPM;  $T_{af} = 1400^{\circ}\text{F}$  AND  $T_{sh} = 1200^{\circ}\text{F}$ ; FIFTH MODE.

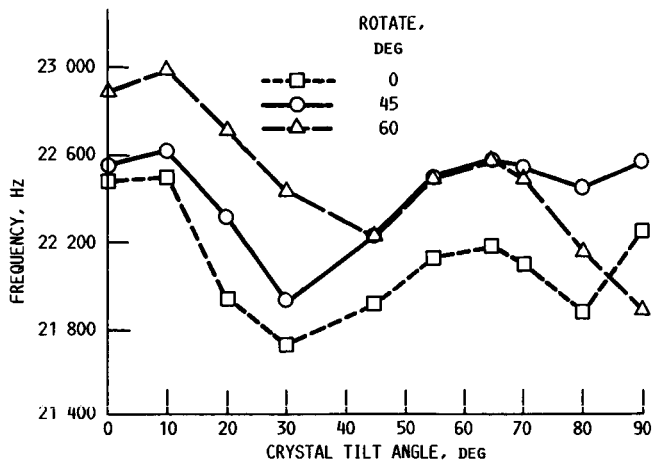


FIGURE 44. - SSME HPFTP FIRST-STAGE BLADE; PWA-1480; 35 000 RPM;  $T_{af} = 1400^{\circ}\text{F}$  AND  $T_{sh} = 1200^{\circ}\text{F}$ ; SIXTH MODE.

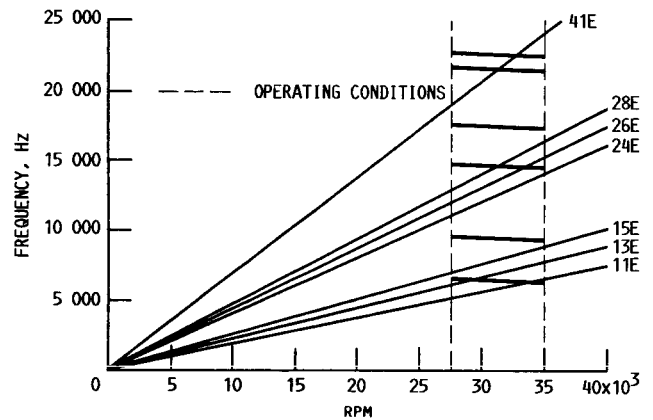


FIGURE 45. - SSME HPFTP FIRST-STAGE BLADE; CAMPBELL DIAGRAM; PWA-1480; SC ORIENTATION: TILT =  $0^{\circ}$  AND ROTATE =  $0^{\circ}$ .

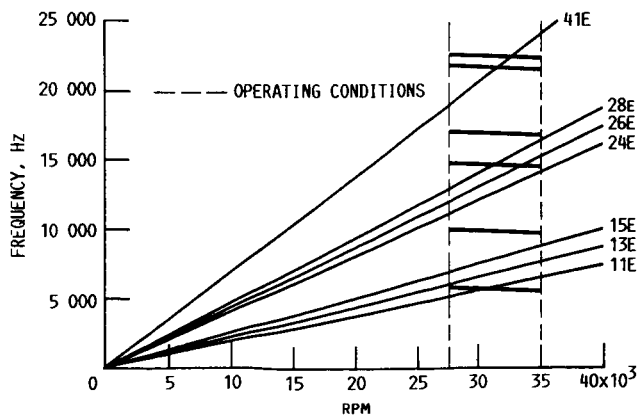


FIGURE 46. - SSME HPFTP FIRST-STAGE BLADE; CAMPBELL DIAGRAM; PWA-1480; SC ORIENTATION: TILT =  $90^{\circ}$  AND ROTATE =  $0^{\circ}$ .

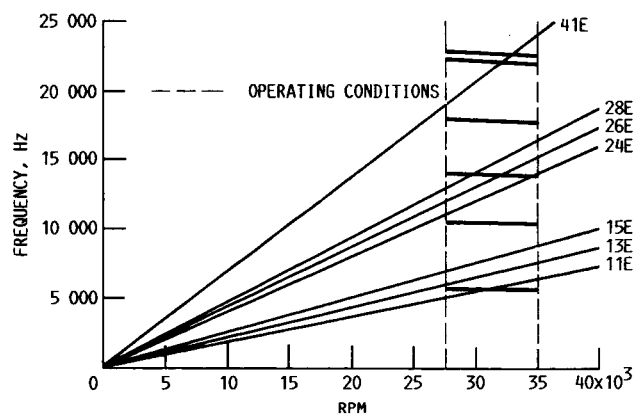


FIGURE 47. - SSME HPFTP FIRST-STAGE BLADE; CAMPBELL DIAGRAM; PWA-1480; SC ORIENTATION: TILT =  $90^{\circ}$  AND ROTATE =  $45^{\circ}$ .

# Report Documentation Page

1. Report No. <b>NASA CR-179644</b>		2. Government Accession No.		3. Recipient's Catalog No.	
4. Title and Subtitle <b>SSME Single Crystal Turbine Blade Dynamics</b>				5. Report Date <b>July 1987</b>	
				6. Performing Organization Code	
7. Author(s) <b>Larry A. Moss and Todd E. Smith</b>				8. Performing Organization Report No. <b>None (E-3671)</b>	
				10. Work Unit No. <b>553-03-04</b>	
9. Performing Organization Name and Address <b>Sverdrup Technology, Inc. Lewis Research Center Cleveland, Ohio 44135</b>				11. Contract or Grant No. <b>NAS3-24105</b>	
				13. Type of Report and Period Covered <b>Contractor Report Final</b>	
12. Sponsoring Agency Name and Address <b>National Aeronautics and Space Administration Lewis Research Center Cleveland, Ohio 44135</b>				14. Sponsoring Agency Code	
15. Supplementary Notes <b>Project Manager, Robert E. Kielb, Structures Division, NASA Lewis Research Center.</b>					
16. Abstract <p>A study was performed to determine the dynamic characteristics of the Space Shuttle main engine (SSME) high pressure fuel turbopump (HPFTP) blades made of single crystal (SC) material. This effort examined both the first and second stage drive turbine blades of the HPFTP. The nonrotating natural frequencies were determined experimentally and analytically. The experimental results of the SC second stage blade were used to verify the analytical procedures. The analytical study examined the SC first stage blade natural frequencies with respect to crystal orientation at typical operating conditions. The SC blade dynamic response was predicted to be less than the directionally solidified (DS) blade. No new engine order interferences were introduced and one was eliminated. Crystal axis orientation optimization indicated the third mode interference will exist at any SC orientation.</p>					
17. Key Words (Suggested by Author(s)) <b>SSME turbopump; Single crystal material; Dynamic characteristics of rotating blades</b>				18. Distribution Statement <b>Unclassified - unlimited STAR Category 39</b>	
19. Security Classif. (of this report) <b>Unclassified</b>		20. Security Classif. (of this page) <b>Unclassified</b>		21. No of pages <b>26</b>	
				22. Price* <b>A03</b>	